Detection of Intensification in Global- and Continental-Scale Hydrological Cycles: Temporal Scale of Evaluation

ALAN D. ZIEGLER AND JUSTIN SHEFFIELD

Environmental Engineering and Water Resources, Princeton University, Princeton, New Jersey

EDWIN P. MAURER

Civil Engineering, University of Washington, Seattle, Washington

BART NIJSSEN

Department of Civil Engineering and Engineering Mechanics, and Department of Hydrology and Water Resources, The University of Arizona, Tucson, Arizona

ERIC F. WOOD

Environmental Engineering and Water Resources, Princeton University, Princeton, New Jersey

DENNIS P. LETTENMAIER

Civil Engineering, University of Washington, Seattle, Washington

(Manuscript received 29 March 2002, in final form 1 August 2002)

ABSTRACT

Diagnostic studies of offline, global-scale Variable Infiltration Capacity (VIC) model simulations of terrestrial water budgets and simulations of the climate of the twenty-first century using the parallel climate model (PCM) are used to estimate the time required to detect plausible changes in precipitation (P), evaporation (E), and discharge (Q) if the global water cycle intensifies in response to global warming. Given the annual variability in these continental hydrological cycle components, several decades to perhaps more than a century of observations are needed to detect water cycle changes on the order of magnitude predicted by many global climate model studies simulating global warming scenarios. Global increases in precipitation, evaporation, and runoff of 0.6, 0.4, and 0.2 mm yr^{-1} require approximately 30–45, 25–35, and 50–60 yr, respectively, to detect with high confidence. These conservative detection time estimates are based on statistical error criteria ($\alpha = 0.05$, $\beta = 0.10$) that are associated with high statistical confidence, $1 - \alpha$ (accept hypothesis of intensification when true, i.e., intensification is occurring), and high statistical power, $1 - \beta$ (reject hypothesis of intensification when false, i.e., intensification is not occurring). If one is willing to accept a higher degree of risk in making a statistical error, the detection time estimates can be reduced substantially. Owing in part to greater variability, detection time of changes in continental P, E, and Q are longer than those for the globe. Similar calculations performed for three Global Energy and Water Experiment (GEWEX) basins reveal that minimum detection time for some of these basins may be longer than that for the corresponding continent as a whole, thereby calling into question the appropriateness of using continental-scale basins alone for rapid detection of changes in continental water cycles. A case is made for implementing networks of small-scale indicator basins, which collectively mimic the variability in continental P, E, and Q, to detect acceleration in the global water cycle.

1. Introduction

Based on plausible scenarios of atmospheric concentrations of greenhouse gases and aerosols, many climate model studies, conducted beneath the umbrella of the Intergovernmental Panel on Climate Change (IPCC), predict mean annual global surface temperature to increase 1.4°–5.8°C by 2100 (Houghton et al. 2001, chapter 9). Predicted warming-associated environmental changes include an increase in global mean sea level of 0.15–0.95 m and alteration of the spatiotemporal patterns of precipitation and soil moisture (Houghton et al. 2001, chapter 9; McCarthy et al. 2001, chapter 4). One alarming manifestation of anthropogenic warming could be an ensuing acceleration of the global hydrological

Corresponding author address: Dr. Alan D. Ziegler, Water Resources Program, Princeton University, CEE E-Quad E-228, Princeton, NJ 08544.
E-mail: adz@princeton.edu

cycle that might lead to increased global precipitation, faster evaporation, and a general exacerbation of extreme hydrologic anomalies, floods, and droughts (Gleick 1989; Easterling et al. 2000; Meehl et al. 2000; Milly et al. 2002). As elucidated by the IPCC (McCarthy et al. 2001, chapter 4), such long-term, large-scale, human-induced changes to global water and energy cycles could interact with natural variability [e.g., the El Niño–Southern Oscillation (ENSO) phenomenon] on daily-to-decadal timescales and may adversely affect social/economic well-being in many regions of the world.

Evidence suggests that some warming-related environmental change can now be detected. The IPCC reports that global average surface temperature has increased over the twentieth century by about $0.6° \pm 0.2°C$ and this increase is likely to have been the largest of any century during the past 1000 yr (Houghton et al. 2001, chapter 2). Daily minimum temperatures over land have been increasing on average by about 0.2°C decade^{-1} over the last 50 yr and maximum temperatures have been increasing by about half that amount leading to a reduction of the daily temperature range (Easterling et al. 1997). With respect to intensification of the global hydrological cycle, a number of studies have looked at changes in the major components. There has been a statistically significant increase of 2% in global land precipitation over the twentieth century (Jones and Hulme 1996; Hulme et al. 1998). However, this change has varied spatially and temporally (Karl and Knight 1998; Doherty et al. 1999). In general, precipitation has increased over most of the mid- and high-latitudes of the Northern Hemisphere and over tropical land areas but has decreased over Northern Hemisphere subtropical land areas. Over the Southern Hemisphere, no comparable changes have been detected at these large scales (Houghton et al. 2001, chapter 2). The consensus among studies of snow cover extent is that there has been an overall reduction in Northern Hemisphere spring snow cover in the latter half of the twentieth century (Hughes and Robinson 1996; Frei et al. 1999; Brown 2000). Increases in streamflow have been noted by several studies (Lettenmaier et al. 1994; Genta et al. 1998; Lins and Slack 1999; Groisman et al. 2001; Zhang et al. 2001, Milly et al. 2002) and can, in general, be related to increases in precipitation, although changes in snow cover may have a dominant effect on the timing and volume of streamflow (Groisman et al. 2001). Soil moisture data for large regions of Eurasia show large positive trends of more than 1 cm decade^{-1} in the top 1 m of soil (Robock et al. 2000) and are coincident with increases in precipitation, despite temperature increases that would normally reduce soil moisture through evapotranspiration. Studies by Golubev et al. (2001) indicate that actual evaporation has increased over most dry regions of the United States and Russia and over the humid maritime regions of the United States during the warm season but has decreased over heavily forested areas. The use of indirect, but better-observed variables, such as diurnal temperature range have also been used to indicate changes in the hydrological cycle. Dai et al. (1999) show that decreases in diurnal temperature range during the last 4–5 decades are consistent with the reported increasing trends in cloud cover and precipitation over many land areas.

In addition to the evidence suggesting global hydrological cycle intensification in the observation record, many general circulation model (GCM) studies of future climates predict substantial increases in globally averaged precipitation and related changes in other water balance variables (e.g., Dai et al. 2001b; also see Easterling et al. 2000; Houghton et al. 2001, chapter 9; Milly et al. 2002). While GCM simulations are not flawless representations of future climates, the similarity in predictions for plausible global warming scenarios by the host of models evaluated in the most recent IPCC assessment is motivation enough for most scientists and policymakers to anticipate some warming-induced changes to the global hydrological cycle. Although it can be argued that it is possible that these models are in error and result in the same incorrect simulations, their ability to provide credible simulations of the climate over broad spatial and temporal scales and the ability of several models to reproduce the major trend in surface air temperature of the twentieth century instill a certain amount of confidence in the their predictions (Houghton et al. 2001, chapter 8).

Over the past couple of decades since the possibility of anthropogenic global warming became apparent, many studies have addressed the problems of 1) detecting warming trends in global and regional temperature records, and/or 2) determining if existing trends are significant and not a component of natural variability (e.g., Wigley and Jones 1981; Bloomfield 1992; Galbraith and Green 1992; Richards 1993; Woodward and Gray 1993; Gordon et al. 1996; Zheng and Basher 1999). Numerous studies have also focused on identifying warming-induced changes to hydrological variables, such as precipitation and river discharge (e.g., Idso and Brazel 1984; Wigley and Jones 1985; Chiew and McMahon 1993; Lettenmaier et al. 1994; Mitosek 1995; Dai et al. 1997; McCabe and Wolock 1997; Karl 1998; Hisdal et al. 2001). While attempts have been made to identify the most suitable statistical models/approaches for detecting trends in the times series of warming-affected climatological variables (e.g., Richards 1993; Woodward and Gray 1993; Zheng and Basher 1999), less effort has been directed at determining timescales needed to detect warming-induced trends. In one example, McCabe and Wolock (1997) examined the likelihood of detecting trends in annual runoff time series for 585 stream gauges in the conterminous United States. Their general conclusion was that unless trend magnitudes were ''large'', ''long'' times series would be needed to detect significantly any trends caused by climate change.

In this work we address the question of what length

of data records is needed to detect changes to the global terrestrial hydrological cycle. We focus on diagnostic studies of global water balance simulations that allow estimation of the time required to detect plausible changes in three major components of terrestrial hydrological cycles, precipitation (P), evaporation (E), and runoff (Q). To do so, we use estimates of ''natural variability,'' derived from global water balance simulations for six continents (Africa, Asia, Europe, North America, Oceania, and South America) to calculate the minimum number of years required to detect the trends in P, E, and Q predicted for one of the global warming scenarios evaluated by the IPCC (Houghton et al. 2001, chapter 9).

2. Data

a. Variable Infiltration Capacity (VIC) model global simulations

The Variable Infiltration Capacity (VIC) model (Liang et al. 1994, 1996) is a macroscale hydrological model that has been used in several large river basin water balance simulations (e.g., Abdulla et al. 1996; Nijssen et al. 1997; Wood et al. 1997; Lohmann et al. 1998a; Maurer et al. 2001). Our diagnostic study examines the 2° global, terrestrial (excluding Greenland and Antarctica) hydrological cycle simulations conducted by Nijssen et al. (2001a). VIC uses forcings derived exclusively from daily precipitation, temperature (minimum and maximum) and wind speed fields to calculate grid cell water balance components, including E, Q, and storage changes (e.g., soil moisture, snow water equivalence). Runoff at each grid cell is routed to the basin outlet using the method of Lohmann et al. (1996, 1998b). Vapor pressure is calculated from dewpoint temperature, which is derived using the method of Kimball et al. (1997). Downward shortwave radiation is calculated based on daily minimum temperature and dewpoint temperature, following Thornton and Running (1999). Net longwave radiation is calculated based on the method of Bras (1990).

Precipitation and temperature forcing data were derived initially from station observations and then extended via stochastic interpolation to areas where meteorological station data were inadequate or unavailable. The resulting daily sequences were scaled to match the means of existing global, monthly time series (Jones 1994; Hulme 1995; Huffman et al. 1997). Daily surface wind speeds were obtained from the joint National Centers for Environmental Prediction and National Center for Atmospheric Research (referred to hereafter as NCEP–NCAR) reanalysis project (Kalnay et al. 1996). Grid cell elevation, soil type, and vegetation characteristics, respectively, were specified using 1) 5-min TerrainBase digital elevation model (DEM; Row et al. 1995) and the land surface mask from Graham et al. (1999); 2) 5-min Food and Agricultural Organization-United Nations Educational and Scientific Cultural Organization (FAO-UNESCO) digital soil map of the world (FAO 1995), combined with the World Inventory of Soil Emissions (WISE) pedon database (Batjes 1995); and 3) the Advanced Very High Resolution Radiometer (AVHRR), 1-km, global land classification from Hansen et al. (2000), which has 12 unique vegetation classes. The remaining soil characteristics, such as porosity, saturated hydraulic conductivity, and the exponent for the unsaturated hydraulic conductivity equation were based on Cosby et al. (1984). Vegetation leaf area index is based on Myneni et al. (1997). Validation of the water balance components for these simulations is reported by Nijssen et al. (2001a,b).

b. Parallel Climate Model simulations

The parallel climate model (PCM) was developed at the National Center for Atmospheric Research and is described by Washington et al. (2000). The PCM results from the coupling in parallel of 1) NCAR Community Climate Model version 3 (CCM3) and land surface model (LSM), 2) the Los Alamos National Laboratory (LANL) Parallel Ocean Program (POP) model, and 3) the sea ice model from the Naval Postgraduate School (NPG). Recent PCM simulations are described by Dai et al. (2001b). For our diagnostic studies, we use output data from PCM simulations B04.10 (PCM version 1.0) and B06.20 (PCM version 1.1). The former is a 300-yr control simulation that we use as an estimate of the natural variability in P, E, and Q. The latter simulation, which we use to estimate trend magnitudes for the twenty-first century, corresponds to ''global warming'' scenario A2 in the most recent IPCC assessments, (Houghton et al. 2001, chapter 6). Scenario A2 is generally regarded as a worst reasonable case scenario that sees a four-to-five-fold increase in CO_2 emissions over the period 2000–99, during which CO_2 concentrations increase from about 350 to over 800 ppm (Houghton et al. 2001, chapter 3). To calculate variability and trend magnitudes we first interpolate the PCM P and E fields (Gaussian grid, 128 $\times$ 64 cells, roughly 2.8°) to our 2° VIC model grid domain (land areas only), and then average over the same grid cells used in the VIC terrestrial water balance simulations. Values of Q for the PCM are not available and so are calculated as residual discharge, $Q = P - E$, by assuming that the year-to-year changes in soil moisture are negligible (cf. Wigley and Jones 1985).

3. Methods

a. Trend detection methodology

We employ a straightforward approach to estimate the minimum number of years required to detect significant trends in continental water cycle variables. This methodology utilizes: 1) the ''natural'' variability in P,

E, and *Q*, as determined from water balance simulations using the VIC model; 2) PCM-predicted trends in *P*, *E*, and *Q* for the twenty-first century for the A2 global warming scenario (Houghton et al. 2001, chapter 6); and 3) statistical equations for determining the probability (β) of committing a type II error in one-sample testing. In all calculations, mean annual values for VIC or PCM grid cells are used.

For the typical hypothesis-testing problem one often compares a null hypothesis (H_0: an event has *not* occurred) with an alternative hypothesis (H_1: an event has occurred). The *t*-test statistic is sometimes used to ''choose'' between H_0 and H_1, particularly for normally distributed data. The probability of choosing H_0 when H_0 is true is $1 - \alpha$; and the probability of choosing H_1 when H_1 is true is $1 - \beta$. These two probabilities are referred to, respectively, as the confidence level of the test and power of the test. Trend detection is a special case of the hypothesis-testing problem, for which the event in question is a trend. Power, which varies with record length, trend magnitude, and the distribution/form of the time series (see Lettenmaier 1975, for a discussion on dependent vs independent series) plays an important role in trend detection because it gives the probability of detecting a trend at a fixed confidence level.

For the trend detection problem, the power of the test is given by the following equation (cf. Lettenmaier 1975):

$$1 - \beta = 1 - F_x\left[W_{1-\alpha/2} - \frac{|\tau_{\min}|}{\text{var}(\hat{\tau})^{1/2}}\right], \quad (1)$$

where $1 - \beta$ is the power of the *t* test; F_x is the cumulative normal distribution; $W_{1-\alpha/2}$ is the normal deviate at cumulative probability $1 - \alpha/2$; $\tau_{\min}$ is the minimum detectable trend per year for the time series in question; and $\text{var}(\hat{\tau})$ is the variance of the time series residual computed over *n* years of observation, calculated as

$$\text{var}(\hat{\tau}) = \frac{\sigma_\varepsilon^2}{\sum_{i=1}^{n} (t_i - \bar{t})^2}, \quad (2)$$

where σ_ε^2 is the estimated variance of the ''noise process'' (assumed to be equal to the sample variance of the time series); values of t_i represent each year of data; and $\bar{t}$ is the mean year.

By rearranging Eq. (1), the minimum number of years ($n_{\min}$) needed to detect a trend for a specified significance level, $1 - \alpha$, and power, $1 - \beta$, can be derived from the left-hand side of the following:

$$\sum_{i=1}^{n} (t_i - \bar{t})^2 = \frac{\sigma_\varepsilon^2}{\tau^2}(W_{1-\alpha/2} - W_\beta)^2, \quad (3)$$

where τ is the trend magnitude, determined herein from the PCM-predicted annual time series; σ_ε^2 is calculated for the VIC water balance simulations (i.e., calculated from the continent-wide average time series); $W_{1-\alpha/2}$ is as above; and W_β is the normal deviate at cumulative probability β. The minimum number of years to detection is calculated by solving iteratively for $n_{\min}$ in Eq. (3).

Within our framework of detection of intensification, α is equivalent to the probability of detecting intensification when there is none and β is equivalent to the probability of not detecting intensification when it is indeed occurring.

b. Trend calculations

The Mann–Kendall test has been used previously to investigate hydroclimatological signals of climate change/variability (e.g., Lettenmaier et al. 1994; Mitosek 1995; Lins and Slack 1999; Hisdal et al. 2001). Based on Kendall's (1975) tau and the work of Mann (1945), the technique, as applied to a time series, tests whether series values tend to increase or decrease as time increases monotonically (cf. Helsel and Hirsch 1992). For two-sided testing of a series with *n* values, we can express the null and alternative hypotheses as

$$H_0: \quad \text{Prob}[Y_j > Y_i] = 0.5; \quad \text{for all } T_j > T_i$$

$$H_1: \quad \text{Prob}[Y_j > Y_i] \neq 0.5,$$

where time series values are denoted by *Y*; *T* is time; $i = 1, 2, \ldots, (n - 1)$; and $j = 2, 3, \ldots, n$.

We calculate the magnitude of a trend [τ in Eq. (3)] as the slope (m) of the Kendall–Theil Robust Line (Theil 1950):

$$y = mt + b, \quad (4)$$

where

$$m = \frac{(y_j - y_i)}{(t_j - t_i)} \quad (5)$$

for all times (t) and data values (y), such that $i < j$, and $i = 1, 2, \ldots, (n - 1)$ and $j = 2, 3, \ldots, n$. In Eq. (4), b is calculated from the median time (t_{median}) and median value (y_{median}) in the time series

$$b = y_{\text{median}} - mt_{\text{median}}. \quad (6)$$

Significance of a trend can be determined from a test statistic *S* that measures the monotonic dependence of *Y* on time:

$$S = \sum_{j=1}^{n-1} \sum_{i=j+1}^{n} \text{sgn}(Y_i - Y_j), \quad (7)$$

where sgn is the sign (positive, negative, zero) of the expression $Y_i - Y_j$. The range of *S* is $\pm n(n - 1)/2$. To test significance, a statistic can be developed that is closely approximated by the standard normal distribution:

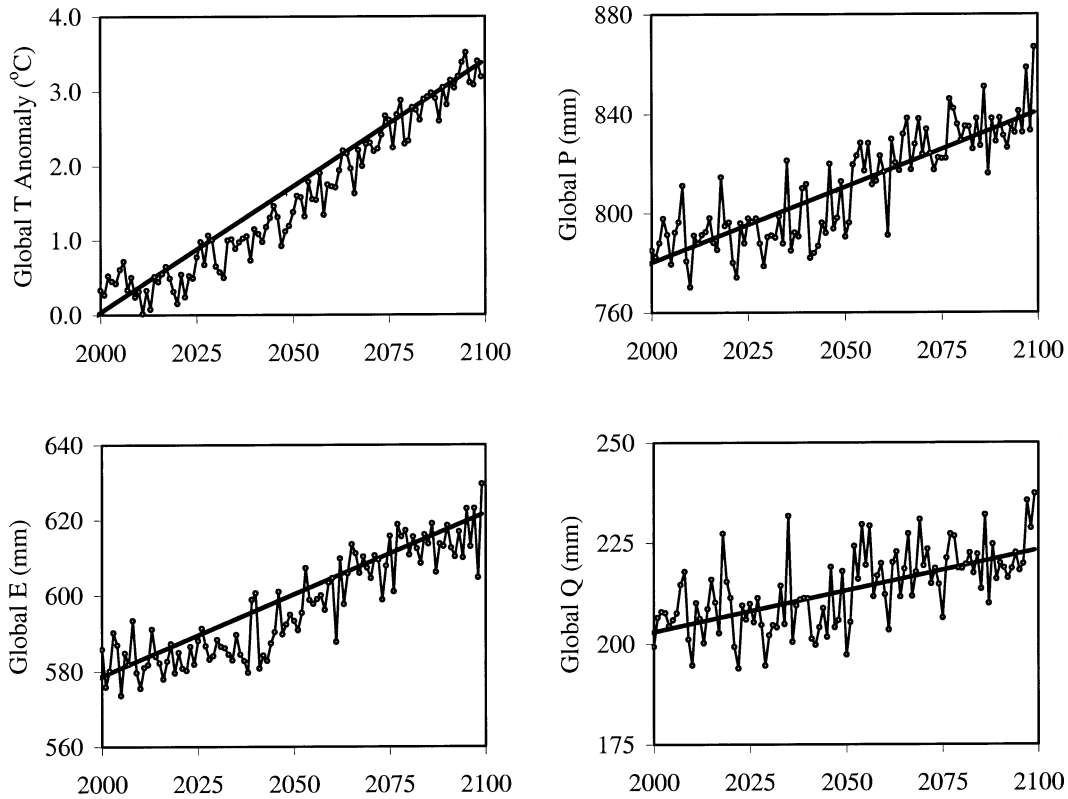

FIG. 1. Yearly global terrestrial surface temperature anomaly, precipitation (P), evaporation (E), and runoff (Q) estimates from PCM model run B06.20 for the period 2000–99 (interpolated to, then averaged over, the VIC 2° × 2° grid domain). The solid line is the Kendall–Theil Robust Line [Eq. (4)], for which each slope is the magnitude of the trend: 0.61, 0.42, and 0.21 mm yr^{-1} for P, E, and Q, respectively; the temperature anomaly trend is 0.033°C yr^{-1}. All trend magnitudes are significant (P-values < 0.0001, Eq. (9)].

$$Z_s = \begin{cases} \dfrac{S-1}{\sigma_S}: & S > 0 \\ 0: & S = 0 \\ \dfrac{S+1}{\sigma_S}: & S < 0 \end{cases} \tag{8}$$

for which σ_S is calculated as

$$\sigma_S = \left[\frac{n(n-1)(2n+5) - \sum_{i=1}^{M} e_i(e_i-1)(2e_i+5)}{18}\right]^{1/2}, \tag{9}$$

where M is the number of tied groups; and e_i is the number of data in the ith tied group. The null hypotheses (H_0) is rejected at significance level α if $|Z_S| > F_x(W_{1-\alpha/2})$, where F_x and $W_{1-\alpha/2}$ are as in Eq. (1). Note, an alternative test should be used for values of n less than 10 (cf. Helsel and Hirsch 1992).

4. Results

a. Predicted trends in P, E, and Q

In Fig. 1, the predicted (PCM run B06.20) land surface temperature anomaly for 2000–99 is shown with the corresponding PCM-predicted global, terrestrial time series of annual P, E, and Q. Each solid line is the Kendall–Theil Robust Line [Eq. (4)], for which the slope is the trend magnitude (τ). The predicted temperature increase of approximately 3.3°C over the 100-yr period initiates increases in P, E, and Q of approximately 60, 40, and 20 mm, respectively, over the same period. All trend magnitudes shown in Fig. 1 are significant [P-values < 0.0001, Eq. (8)]. In Table 1, τ values for P, E, and Q (i.e., those shown in Fig. 1) are reported for the collective land areas of the world (excluding Greenland and Antarctica) and for each continent. Increases in terrestrial precipitation and evaporation are predicted for nearly all continents for the 100-yr period, beginning in 2000 (also see Dai et al. 2001a). The largest predicted precipitation increases are for Asia and North America ($\geq$0.71 mm yr^{-1}); the smallest is for Africa (0.24 mm yr^{-1}). Africa and Oceania have the smallest predicted evaporation increase (0.31–0.32 mm yr^{-1}); for all other continents, E is predicted to increase by a range of 0.40–0.46 mm yr^{-1}. The smallest predicted runoff (again, $Q = P - E$) change is for Africa (<-0.10 mm yr^{-1}). Asia, which has the highest predicted increase of P (0.77 mm yr^{-1}), also has the greatest predicted increase in Q ($>$0.30 mm yr^{-1}).

TABLE 1. Estimated continental and global terrestrial trends (τ) for precipitation (P), evaporation (E) and runoff ($Q = P - E$), as predicted by run B06.20 for 2000–99; variances (σ^2) for P, E, and Q, determined from VIC simulations of terrestrial water balance (Nijssen et al. 2001a); and min years required to detect significantly ($\alpha = 0.05$; $\beta = 0.10$) the estimated τ, given σ^2_{VIC}.

	Variable	Units	Africa	Asia	Europe	North America	Oceania	South America	World
	τ	mm yr^{-1}	0.24	0.77	0.62	0.71	0.45	0.63	0.61
P	σ^2_{VIC}	mm	2421	357	751	433	2512	2912	260
	$n_{\text{min VIC}}$	yr	173	43	63	48	115	97	45
	τ	mm yr^{-1}	0.32	0.46	0.45	0.45	0.31	0.40	0.43
E	σ^2_{VIC}	mm	609	83	147	70	831	337	63
	$n_{\text{min VIC}}$	yr	90	37	45	35	103	65	35
	τ	mm yr^{-1}	−0.09	0.31	0.14	0.26	0.14	0.24	0.20
Q	σ^2_{VIC}	mm	283	162	589	217	840	1609	119
	$n_{\text{min VIC}}$	yr	162	60	154	73	177	152	71

b. Variability in P, E, and Q

Variances of terrestrial P, E, and Q for the VIC dataset are listed for each continent and combined land areas of the world in Table 1. In general, the three continents located predominantly in the Southern Hemisphere (i.e., Africa, Oceania, and South America) have the highest variances, particularly for variables P and E. Variance estimates for terrestrial land areas (i.e., the world in Table 1) are smaller than those of any individual continent, owing to aggregating over a larger spatial area (i.e., all the grid cells comprising the six continents).

c. Minimum detection time

Table 1 lists the minimum years (n_{min}) needed to detect significantly the continental and global P, E, and Q trends predicted by PCM run B06.20 for the period 2000–99. The n_{min} values are computed via Eq. (3) using variances calculated from the VIC forcing/output data (Table 1), and the trend magnitude values (τ) also listed in Table 1. Owing to large estimated variability in water balance variables, Africa, Oceania, and South America generally require the longest data records to detect the predicted τ values. For the opposite reason (i.e., low variability), detection time for global terrestrial changes in P, E, and Q (world, Table 1) is generally shorter than for any individual continent.

5. Discussion

a. Trend detection time

Assuming that the VIC offline forcing data and simulation output provide realistic approximations of the natural variability in continental-scale P, E, and Q [this is demonstrated by Nijssen et al. (2001a) to be a reasonable assumption], data records having lengths on the order of 35–70 yr are needed to detect significant changes in global terrestrial P, E, and Q that might be caused by a warming-induced intensification in the global hydrological cycle (i.e., world, Table 1). For example, the 0.61 mm yr^{-1} increase in global land precipitation predicted by the PCM simulation, requires 45 yr of observation data to detect significantly (using the criteria $\alpha = 0.05$ and $\beta = 0.10$). The 0.43 and 0.20 mm yr^{-1} predicted changes in global land E and Q require 35 and 71 yr of data, respectively, to detect significantly.

In comparison with the global estimates, longer records spanning a few decades to more than a century are needed to detect predicted changes in P, E, and Q for individual continents. Africa, Oceania, and South America have n_{min} values exceeding 100 yr for some, but not all, of the three hydrological variables considered. The long detection times result from high variability in the annual time series (e.g., Oceania P), small predicted trend magnitudes (e.g., Africa Q), or both (e.g., Africa P). Detection times for evaporation changes are less than those for P and Q because the variances are comparatively smaller and the predicted trends are substantial, although less than those for P. In general, the following relationship holds for both the n_{min} estimates: $n_{\text{min}}(E) < n_{\text{min}}(P) < n_{\text{min}}(Q)$ (with Africa being the lone exception).

It should be noted that the detection time depends on the magnitude of the trends and is thus dependent on the GCM used. A comparison of predicted changes in global temperature and precipitation for the A2 scenario for a range of models is given by the IPCC (Houghton et al. 2001, chapter 9) and shows that the PCM predictions lie somewhere in the middle of the range of other models. Assuming that this is also true for global land precipitation, detection times based on the PCM-predicted trends would fall within the range of values calculated using a number of different models.

b. Risk acceptance

An important factor affecting the time required to detect significant changes in global water cycle variables is the level of risk one is willing to accept in making the determination. For instance, the estimates of n_{min} reported in Table 1 are calculated using low values for the probability of making type I and II errors ($\alpha = 0.05$, $\beta = 0.10$, respectively). These conservative criteria equate, respectively, to ''low risk'' in (a) detecting

TABLE 2. Values of n_{min} for precipitation (P), evaporation (E), and runoff (Q) calculated using the standard normal deviates for various values of α and β [from Eq. (3)] shown for the world only. PCM-predicted trend magnitude (τ) and VIC-derived variances used in these min detection time calculations are those in Table 1.

		β				
		0.01	0.05	0.10	0.25	0.50
	0.01	58	52	49	44	37
	0.05	53	47	45	38	31
P α	0.10	51	44	41	35	28
	0.25	47	41	38	31	24
	0.50	42	35	31	25	15
	0.01	45	41	38	34	29
	0.05	42	37	35	30	25
E α	0.10	40	35	32	28	22
	0.25	37	32	29	25	18
	0.50	33	28	25	19	12
	0.01	92	83	78	73	59
	0.05	85	76	71	62	51
Q α	0.10	81	71	66	57	45
	0.25	76	66	60	51	38
	0.50	67	57	51	40	25

change when it is not occurring or (b) not detecting change when it is occurring. In Table 2 we show results for the world only that indicate how detection time for each variable decreases as risk acceptance increases (i.e., as α and β increase). The value in the upper-left-hand corner corresponds to using α and β values of 0.01 (i.e., high confidence of not committing either a type I or II error). The values in row 2 ($\alpha = 0.05$), column 3 ($\beta = 0.10$) are the estimates reported in Table 1. As we allow α and β to increase (i.e., increase the risk of making a detection error), the time to detect significant changes in P, E, and Q reduces. Values of n_{min} are encountered that may be more conducive to answering critical questions regarding global warming (i.e., is it or is it not affecting the global and/or continental hydrological cycles?), and in making prompt policy decisions that may mitigate the affects. However, one must keep in mind that these shorter detection times come with the associated cost of higher risk in making the determination.

c. Uncertainty in GCM-derived estimates of variance

One downside in our methodology is that the VIC forcing/simulation data fields span a short period (14 yr). Variability estimates for E and Q are computed from model output, rather than from reliable observations, which do not currently exist at this resolution (i.e., 2°) for all terrestrial areas; the precipitation data is, however, derived from observations. Ideally, we would like to base the variance estimates on decades to centuries of data. For all variables, reliable, complete, lengthy datasets of this nature do not exist at any resolution. One plausible way of approaching the problem, however, is to estimate variability from P, E, and Q fields, extracted from multicentury-long GCM control runs.

In Table 3, variances in P, E, and Q are shown for PCM version 1.0 simulation B04.10, a 300-yr control simulation. Although PCM version 1.0 and 1.1 runs (1.1 is used to calculate the trends herein) are not directly intercomparable, the version 1.0 run is adequate for determining the variability of the water balance variables (http://www.cgd.ucar.edu/pcm/). Also shown in Table 3 are 1) the predicted trend magnitudes for 2000–99 (i.e., those shown in Table 1); 2) the ratio of the PCM-derived variances to those of VIC ($\sigma^2_{PCM}/\sigma^2_{VIC}$); 3) minimum de-

TABLE 3. Estimated continental and global terrestrial trends (τ) for precipitation (P), evaporation (E), and runoff ($Q = P - E$), as predicted by the PCM run B06.20 for 2000–99 (from Table 1); variances (σ^2) for P, E, and Q, determined from a 300-yr PCM control simulation (run B04.10); ratio of the PCM- and VIC-derived variances for each variable; min years required to detect significantly [$\alpha = 0.05$; $\beta = 0.10$; Eq. (3)] the estimated trend τ, given the variance determined in the PCM simulation; and ratio of the PCM-derived detection time to that determined using the VIC variance.

	Variable*	Units	Africa	Asia	Europe	North America	Oceania	South America	World
	τ	mm yr^{-1}	0.24	0.77	0.62	0.71	0.45	0.63	0.61
	σ^2_{PCM}	mm	796	239	574	354	3743	1640	92
P	$\sigma^2_{PCM}/\sigma^2_{VIC}$	—	0.33	0.67	0.76	0.82	1.49	0.56	0.35
	$n_{min\ PCM}$	yr	119	37	58	45	132	80	32
	$n_{min\ PCM}/n_{min\ VIC}$	—	0.69	0.88	0.91	0.93	1.14	0.83	0.71
	τ	mm yr^{-1}	0.32	0.46	0.45	0.45	0.31	0.40	0.43
	σ^2_{PCM}	mm	166	58	173	81	2057	296	24
E	$\sigma^2_{PCM}/\sigma^2_{VIC}$	—	0.27	0.70	1.17	1.15	2.47	0.88	0.38
	$n_{min\ PCM}$	yr	59	32	48	37	139	62	25
	$n_{min\ PCM}/n_{min\ VIC}$	—	0.65	0.89	1.05	1.05	1.35	0.96	0.72
	τ	mm yr^{-1}	−0.09	0.31	0.14	0.26	0.14	0.24	0.20
	σ^2_{PCM}	mm	347	119	367	200	668	777	41
Q	$\sigma^2_{PCM}/\sigma^2_{VIC}$	—	1.23	0.73	0.62	0.92	0.80	0.48	0.35
	$n_{min\ PCM}$	yr	173	54	132	71	164	119	50
	$n_{min\ PCM}/n_{min\ VIC}$	—	1.07	0.90	0.85	0.97	0.93	0.79	0.71

* Subscripts for n_{min} reflect which variance estimate (VIC or PCM) was used in the calculation.

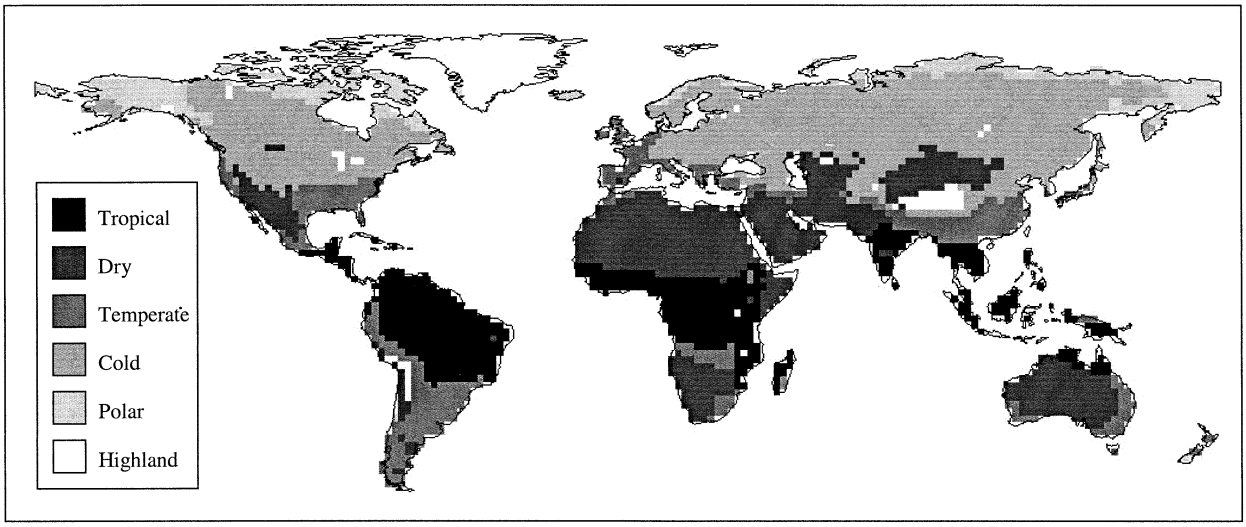

FIG. 2. Köppen climate classes for land areas except Greenland and Antarctica. The 31 subclasses in the Köppen classification have been lumped into six major classes. Asia plays host to 25 of the 31 Köppen subclasses.

tection time predictions using the PCM-derived variances ($n_{\text{min\_PCM}}$); and 4) the ratio of the PCM-derived n_{min} estimates to those calculated using the VIC-derived variances ($n_{\text{min\_PCM}}/n_{\text{min\_VIC}}$).

The greatest differences between σ^2_{VIC} and σ^2_{PCM} are for Africa, Oceania, and South America, the three continents located predominantly in the Southern Hemisphere. The σ^2_{PCM} estimates tend to be smaller than those for VIC, with exceptions for Africa (*Q* only), Europe (*E* only), North America (*E* only) and Oceania (*P* and *E*). The differences for Africa, Europe, and North America, however, are small. In most cases, higher variability estimates make the $n_{\text{min\_VIC}}$ values longer than the PCM-based $n_{\text{min\_PCM}}$ values. One is tempted to use simply the $n_{\text{min\_VIC}}$ and $n_{\text{min\_PCM}}$ to define a range for trend detection time. Table 3 shows the implications of doing so: detection time estimates differ by as much as $\pm 35\%$, with the $n_{\text{min\_PCM}}$ estimates being shorter for the majority of the variables and continents. While a range of estimates may be practical for policy-making decisions, we have confidence in the VIC-derived values because (a) the *P* data field is derived from observations (Nijssen et al. 2001a) and (b) the other variables have been validated for large global river systems (Nijssen et al. 2001a). Similarly, Maurer et al. (2001) showed VIC produced more realistic variance estimates than typical GCM runs for mean water cycle elements over the continents.

d. Climate diversity

Of all the continents, the variance estimates for Asia *P*, *E*, and *Q* are most similar to those calculated for all global terrestrial areas as a whole (world, in Table 1). This similarity is related, in part, to Asia occupying a large landmass (approximately 36% of the global area in the VIC model domain) that spans a large range of latitudinal zones (from 7°S to 77°N in the VIC domain). Asia also hosts most of the major climate systems that comprise the global system. This can be seen in Fig. 2, where the world is divided into Köppen climate classes (see appendix), which are computed using *P, T,* and elevation variables for $2^\circ \times 2^\circ$ grid cells in the VIC domain. Using areal percentages for each class, we can assess how ''similar'' each of the continents is to the world as a whole by calculating the root-mean-square error (rmse):

$$\text{rmse} = \left[\frac{1}{31}\sum_{\text{class=Af}}^{H}(\text{Area}_{\text{continent,class}} - \text{Area}_{\text{world,class}})^2\right]^{1/2}, \tag{10}$$

where class refers to the 31 subclasses of the Köppen classification and area is the fractional area of each subclass on any given continent or the world as a whole. The fractional areas for the six major climate classes and rmse values are given in Table 4. The rmse values show that the Asian continent, which contains 25 out of 31 subclasses, is more similar to the world than the other continents by this simplistic measure. Small annual variability for the Asian water balance variables (as compared with the other continents), therefore, results from the damping of seasonal extremes associated with relatively small regions (e.g., monsoon rainfall, polar winters vs tropical winters) when aggregating over the whole of Asia. Similarly, this dampening occurs when calculating the variances for all terrestrial lands areas of the world as a whole. In this respect, Asia, more than any other individual continent, ''mimics'' the variability in the global hydrological cycle.

TABLE 4. Fractional area of each of the six major Köppen Climate classes for the continents and the world (land areas excluding Greenland and Antarctica) and rmse in the fractional area of Köppen subclasses between each continent and the world.

Class	Description*	Number of subclasses	Fractional area						
			World	Africa	Asia	Europe	North America	Oceania	South America
A	Tropical	3	16.7	35.6	6.7	0.0	2.7	14.1	59.2
B	Dry	4	23.8	57.9	21.1	1.4	8.0	64.9	6.0
C	Temperate	9	12.6	6.5	8.4	17.9	11.1	20.5	31.8
D	Cold	12	36.7	0.0	52.0	75.6	52.4	0.0	0.0
E	Polar	2	10.2	0.0	11.8	5.1	25.8	0.5	28.0
H	Highland	1	0.0	0.0	0.0	0.0	0.0	0.0	0.0
	Rmse [Eq. (11)]			0.08	0.02	0.09	0.05	0.07	0.07

* Criteria for classification and details of subclasses are listed elsewhere (Critchfield 1983; Table 6.6).

e. GEWEX large-scale observation basins

Currently there are several large-scale experimental watershed studies conducted within the framework of the Global Energy and Water Experiment (GEWEX) that are dedicated, in part, to understanding variations in regional hydrological processes and their response to environmental changes, including those associated with anthropogenic warming. GEWEX objectives likely include gathering data useful for detection of intensification of the global water cycle (cf. Morel 2001). Because measuring/monitoring water cycle variables for entire continents is not feasible at this time, GEWEX experimental basins are potentially the most important data gathering sources currently available for detecting intensification of the global water cycle. Rapid detection, however, will depend greatly on the natural variability of the water cycle variables within these basins and also on the actual hydrological changes that will occur therein.

TABLE 5. Estimated continental and global terrestrial trends (τ) for precipitation (P), evaporation (E), and runoff ($Q = P - E$), as predicted by PCM run B06.20 for 2000–99 for three GEWEX basins in North and South America; estimated variances (σ^2) for P, E, and Q, determined from VIC simulations of terrestrial water balance (Nijssen et al. 2001a); comparison of GEWEX basin variances with that of each corresponding continent; min years required to detect significantly ($\alpha = 0.05$; $\beta = 0.10$) the estimated trend τ, given the variance determined in the VIC simulation; and comparison of n_{min} values for each GEWEX basin with that of each corresponding continent.

	Variable	Units	Amazon	Mackenzie	Mississippi
P	τ	mm yr^{-1}	1.48	0.98	0.66
	τ vs continent[a]		2.3	1.4	0.9
	σ^2_{VIC}	mm	9117	911	5551
	σ^2 vs continent[b]	—	3.1	2.1	12.8
	n_{min_VIC}	yr	81	50	116
	n_{min} vs continent[c]	—	0.83	1.03	2.43
E	τ	mm yr^{-1}	0.69	0.39	0.78
	τ vs continent[a]		1.7	0.9	1.7
	σ^2_{VIC}	mm	869	247	1041
	σ^2 vs continent[b]	—	2.6	3.5	14.8
	n_{min_VIC}	yr	61	59	60
	n_{min} vs continent[c]	—	0.95	1.66	1.70
Q	τ	mm yr^{-1}	0.83	0.56	−0.11
	τ vs continent[a]		3.5	2.1	−0.4
	σ^2_{VIC}	mm	4788	157	1475
	σ^2 vs continent[b]	—	3.0	0.7	6.8
	n_{min_VIC}	yr	96	40	253
	n_{min} vs continent[c]	—	0.63	0.54	3.45

[a] Values for τ vs continent are calculated as $\tau_{GEWEX}/\tau_{continent}$.
[b] Values for σ^2 vs continent are calculated as $\sigma^2_{VIC,GEWEX}/\sigma^2_{VIC,continent}$.
[c] Values for n_{min} vs continent are calculated as $n_{min\ VIC,GEWEX}/n_{min\ VIC,continent}$.

In Table 5 we report n_{min} values for the three GEWEX experimental basins in North and South America (shown in Fig. 3): (a) Mississippi River basin [GEWEX Continental-Scale International Project (GCIP)]; (b) Amazon River basin [Large Scale Biosphere–Atmosphere Experiment in the Amazon (LBA)]; and (c) Mackenzie River basin [Mackenzie GEWEX Study (MAGS)]. Values of τ and σ^2 are calculated from VIC and PCM forcing/output fields using the same methodology as those shown in Table 1. Variances in P, E, and Q for the GEWEX basins are generally greater than those for each corresponding continent, which occupies a greater landmass. Again this results from aggregating annual grid cell values over larger land areas (i.e., the entire North or South American continent), such that the influence of small-scale extrema is checked by larger zones of similar climatology or by cells having opposing climate signals.

Holding trend magnitudes constant, the higher variances for P, E, and Q in the three GEWEX basins should equate to longer n_{min} values than were calculated for the continents as whole. As seen in Table 4, however, the PCM-predicted τ values for GEWEX basins are not constant; they differ substantially from those for each corresponding continent. Minimum detection times for some of the GEWEX basins (and for some water balance variables) are therefore shorter than those for the corresponding continental values (e.g., the Amazon basin for all variables, Table 5). As expected, however, n_{min} values for the Mississippi basin are roughly 2–3 times longer than those calculated for the North American continent. The variance estimates for all Mississippi basin variables were 7–13 times higher than those for North America. In the other North American basin, the

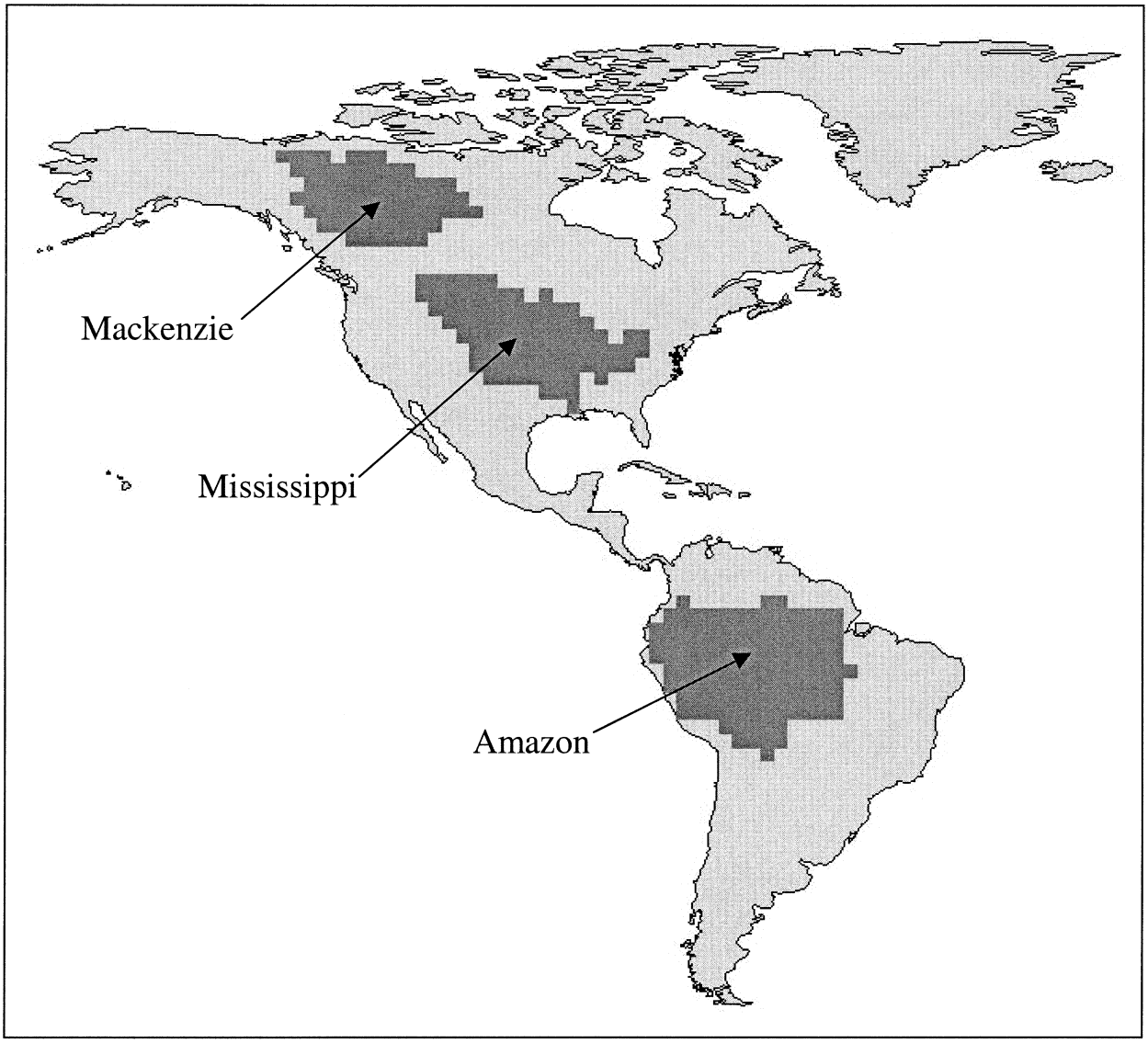

FIG. 3. Locations of three GEWEX experimental basins in North and South America: Mississippi River basin (GCIP); Amazon River basin (LBA); and Mackenzie River basin (MAGS). Basin boundaries are defined by the 2° × 2° VIC grid cells representing each GEWEX watershed.

Mackenzie, n_{min} values for E and Q are within ±66% of those calculated for the continent; the P n_{min} values, however, are practically identical. Owing to the relative closeness between MAGS and North American n_{min} values, the Mackenzie basin may therefore be more useful than GCIP for rapid detection of continental-scale water cycle intensification. In this respect, the LBA experiment may be the most useful, as n_{min} values are 5%–37% shorter than those for the entire South American continent.

f. A case for small-scale indicator basins

Using GEWEX projects for detection of changes in a continental water cycle is attractive because these large continental-scale watersheds cover a significant part of their respective continents. To do so, however, we must assume that changes occurring in the basin (i.e., the trend magnitudes realized) are representative of those occurring on the continent as a whole. Comparison of the PCM-predicted τ values for the Mackenzie and Mississippi basins echoes what numerous other GCM studies of global warming suggest: the ensuring hydrological cycle changes will vary from region to region, with some areas showing various degrees of increases and decreases. Thus, the trend for any one basin (up to some threshold spatial scale) could differ substantially from that occurring for the continent as a whole (e.g., again, the predicted τ values for the Amazon are 1.7–3.5 times higher than those for South America, Table 5).

Although GEWEX sites are arguably the most sophisticated large-scale basin monitoring systems currently available for detecting water cycle intensification (Morel 2001), we are currently investigating the possibility of selecting within each continent several small-scale (e.g., on the order of 2° or smaller) basins, for which the natural variability in water balance variables *collectively* mimics that of the corresponding continent. We stress collectively, because individual small-scale basins will generally have greater variability than the larger-scale basins (as shown above for continents vs the globe and for GEWEX basins vs corresponding continents). The higher variability will almost certainly result in longer detection time, unless observed trends are themselves substantially larger as is the case with the LBA project (Table 5).

It may be that these ''indicator'' basins are best selected based on climatic criteria (e.g., Köppen system or other) to ensure that the continental climate diversity is preserved. Monitoring indicator basins for water cycle intensification may be more feasible than monitoring continental water cycles as a whole. This collective network of basins may also be more representative of continental changes than are larger-scale basins having very different natural variabilities.

g. Influence of measurement error

Measurement errors are inherent in the Nijssen et al. (2001a) VIC precipitation forcings. In this work, however, we were not able to assess the extent that measurement errors contribute to greater estimates of natural variability. In well-instrumented areas, such as North America, the measurement error influence is probably small, or at least acceptable for the hydrological acceleration detection methodology we propose. If this is true, denser observation networks, regardless of being a part of a collective network of indicator basins, may not contribute substantially to better detection capability. For continents such as Africa, the density of the climate observation network is so sparse that the effects of measurement error on increasing variability estimates likely hinders our ability to detect rapidly continental changes in hydrological cycle variables. Additional basins measuring P should therefore improve estimates of ''natural'' variability, which in turn would lead to better $n_{\min}$ estimates. In addition, satellite-augmented products akin to the Global Precipitation Climatology Project (WCRP 1990; Huffman et al. 1997) and Xie and Arkin (1997) datasets could prove useful in calculating natural variability and detecting trends in precipitation, especially as remote sensing data analysis techniques improve.

The other hydrological variables, E and Q, present problems for detection of acceleration in the global hydrological cycle. Evaporation is measured relatively poorly at any scale. Diagnostic studies of water balance simulations (such as the VIC simulations considered above) may therefore be the only suitable approach to estimating E variability at this time. Such E estimates may be quite reasonable when precipitation is derived from measurements and Q is validated using observations. Streamflow measurement is, however, complicated by water management issues (e.g., dams, water diversion). With this difficulty in mind, it might be better to first concentrate on estimating accurately the water management effects at the continental scale, then deduce the natural flows, rather than implement several small-scale indicator watersheds to measure streamflow directly.

6. Conclusions

Using 1) estimates of natural variability in precipitation, evaporation, and discharge, and 2) a parallel climate model simulation of the IPCC (Houghton et al. 2001, chapter 6) global warming scenario A2, we determined that data records having lengths on the order of 35–70 yr are needed to detect significantly changes in global terrestrial P, E, and Q that might be caused by a warming-induced intensification in the global hydrological cycle. Longer records are generally needed to detect predicted changes in P, E, and Q at the continental scale. Although our study is based on trends that are predicted to occur over the course of the twenty-first century, one may not need to wait until 2030–60 to detect changes in the global hydrological cycle. For instance, if the trends are a continuation of phenomena that have been occurring over the last few decades—a time period for which we may already have reliable observations (e.g., for precipitation, Global Precipitation Climatology Project, WCRP 1990; Huffman et al. 1997)—we may, therefore, be able to detect with confidence acceleration in some water balance variables by the end of this decade or the next. If any realized global warming is less than that predicted by the PCM simulations used herein, the trend magnitudes for P, E, and Q would likely be less than those we used in calculating minimum detection time; and therefore, detection time would be longer.

Minimum time required to detect water cycle intensification is inherently controlled by the level of risk that one is willing to take in making the determination. This in itself is vexing because it allows policymakers to manufacture estimates that support a wide range of political agendas. Our estimates are made using conservative, low-risk probabilities of making type I and type II errors during detection ($\alpha = 0.05$, $\beta = 0.10$, respectively). In general, the low-risk values that we report seem to be in line with the current political attitude toward global warming in the United States (i.e., more time is needed for detection before making radical steps toward mitigating the impacts of global warming); higher risk values (i.e., less time required for detection) seem to reflect European sentiment.

Ultimately, detection of global/continental scale hy-

drological cycle acceleration depends on gathering data at a scale appropriate for estimating natural variability and detecting changes. Owing to the current difficulty in obtaining continental-scale data, especially evaporation, the need for improved measurement technology, including satellite remote sensing techniques, becomes apparent. Large-scale hydrological assessment programs such as GEWEX, which are a vital first step in assessing/detecting global hydrological changes, may not alone be sufficient to detect rapidly changes to continental-scale hydrological cycles. It may be beneficial to identify several small-scale (e.g., on the order of 2° or smaller) basins within each continent, for which the natural variability in water balance variables ''collectively mimics'' that of each respective continent. The time to detect hydrological changes occurring in such a collective network of basins may therefore be more representative of the time required to detect the associated continental changes (work in progress).

Acknowledgments. This work is supported by NASA Grants NAG5-9414 and NAG5-9486. PCM data were downloaded with permission from the UCAR website (http://www.cgd.ucar.edu/pcm/). Two anonymous reviewers gave valuable comments on the manuscript.

APPENDIX

Köppen Climate Classification System

The original Köppen Climate Classification, developed in 1918 by Wladimir Köppen, divides terrestrial areas into five major climatic categories using temperature and precipitation criteria: (A) tropical climates; (B) dry climates; (C) warm temperature rainy climates and mild winters; (D) cold forest climates and severe winters; (E) polar climates. Herein we use a modified classification, in which a sixth major class (H, highland climates) is added (cf. Critchfield 1983). The Köppen system represents one of many schemes developed to represent areas of similar climatic conditions. We use it in this work as a simple index of the diversity of climatic zones within the continents and the world.

REFERENCES

Abdulla, F. A., D. P. Lettenmaier, E. F. Wood, and J. A. Smith, 1996: Application of a macroscale hydrologic model to estimate the water balance of the Arkansas–Red River Basin. *J. Geophys. Res.,* **101,** 7449–7459.

Batjes, N. H., 1995: A homogenized soil data file for global environmental research: A subset of FAO, ISRIC and NCRS profiles. Tech. Report, International Soil Reference and Information Centre (ISRIC), Wageningen, Netherlands, 43 pp.

Bloomfield, P., 1992: Trends in global temperature. *Climatic Change,* **21,** 1–16.

Bras, R. L., 1990: *Hydrology: An Introduction to Hydrologic Science.* Addison-Wesley, 643 pp.

Brown, R. D., 2000: Northern Hemisphere snow cover variability and change, 1915–97. *J. Climate,* **13,** 2339–2355.

Chiew, F. H. S., and T. A. McMahon, 1993: Detection of trend or change in annual flow in Australian rivers. *Int. J. Climatol.,* **13,** 643–653.

Cosby, B. J., G. M. Hornberger, R. B. Clapp, and T. R. Ginn, 1984: A statistical exploration of the relationships of soil moisture characteristics to the physical properties of soils. *Water Resour. Res.,* **20,** 682–690.

Critchfield, H. J., 1983: *General Climatology.* 4th ed. Prentice Hall, 453 pp.

Dai, A., I. Y. Fung, and A. D. Del Genio, 1997: Surface observed global land precipitation variations during 1900–88. *J. Climate,* **10,** 2943–2962.

——, K. E. Trenberth, and T. R. Karl, 1999: Effects of clouds, soil moisture, precipitation, and water vapor on diurnal temperature range. *J. Climate,* **12,** 2451–2473.

——, G. A. Meehl, W. M. Washington, T. M. L. Wigley, and J. A. Arblaster, 2001a: Ensemble simulation of twenty-first century climate changes: Business-as-usual versus CO_2 stabilization. *Bull. Amer. Meteor. Soc.,* **82,** 2377–2388.

——, T. M. L. Wigley, B. A. Boville, J. T. Kiehl, and L. E. Buja, 2001b: Climates of the twentieth and twenty-first centuries simulated by the NCAR climate system model. *J. Climate,* **14,** 485–519.

Doherty, R. M., M. Hulme, and C. G. Jones, 1999: A gridded reconstruction of land and ocean precipitation for the extended Tropics from 1974–1994. *Int. J. Climatol.,* **19,** 119–142.

Easterling, D. R., and Coauthors, 1997: Maximum and minimum temperature trends for the globe. *Science,* **277,** 364–367.

——, G. A. Meehl, C. Parmesan, S. A. Changnon, T. R. Karl, and L. O. Mearns, 2000: Climate extremes: Observations, modeling, and impacts. *Science,* **289,** 2068–2074.

FAO, 1995: *Digital Soil Map of the World and Derived Soil Properties (Version 3.5).* FAO Land and Water Digital Media Series, CD-ROM.

Frei, A., D. A. Robinson, and M. G. Hughes, 1999: North American snow extent: 1900–1994. *Int. J. Climatol.,* **19,** 1517–1534.

Galbraith, J. W., and C. Green, 1992: Inference about trends in global temperature data. *Climatic Change,* **22,** 209–221.

Genta, J. L., G. Perez-Iribarren, and C. R. Mechoso, 1998: A recent increasing trend in the streamflow of rivers in southeastern South America. *J. Climate,* **11,** 2858–2862.

Gleick, P. H., 1989: Climate change, hydrology, and water resources. *Rev. Geophys.,* **27,** 329–344.

Golubev, V. S., J. H. Lawrimore, P. Y. Groisman, N. A. Speranskaya, S. A. Zhuravin, M. J. Menne, T. C. Peterson, and R. W. Malone, 2001: Evaporation changes over the contiguous United States and the former USSR: A reassessment. *Geophys. Res. Lett.,* **28,** 2665–2668.

Gordon, A. H., J. A. T. Bye, and R. A. D. Byron-Scott, 1996: Is global warming climate change? *Nature,* **380,** 478.

Graham, S. T., J. S. Famiglietti, and D. R. Maidment, 1999: Five minute, 1/2°, and 1° data sets of continental watersheds and river networks for use in regional and global hydrologic and climate system modeling studies. *Water Resour. Res.,* **35,** 583–587.

Groisman, P. Y., R. W. Knight, and T. R. Karl, 2001: Heavy precipitation and high streamflow in the contiguous United States: Trends in the twentieth century. *Bull. Amer. Meteor. Soc.,* **82,** 219–246.

Hansen, M. C., R. S. Defries, J. R. G. Townshend, and R. Sohlberg, 2000: Global land cover classification at 1km spatial resolution using a classification tree approach. *Int. J. Remote Sens.,* **21,** 1331–1364.

Helsel, D. R., and R. M. Hirsch, 1992: *Statistical Methods in Water Resources.* Elsevier, 522 pp.

Hisdal, H., K. Stahl, L. M. Tallaksen, and S. Demuth, 2001: Have streamflow droughts in Europe become more severe or frequent? *Int. J. Climatol.,* **21,** 317–333.

Houghton, J. T., Y. Ding, D. J. Griggs, M. Noguer, P. J. van der Linden, and D. Xiaosu, Eds., 2001: *Climate Change 2001: The Scientific Basis.* Cambridge University Press, 944 pp.

Huffman, G. J., and Coauthors, 1997: The Global Precipitation Cli-

matology Project (GPCP) Combined Precipitation dataset. *Bull. Amer. Meteor. Soc.,* **78,** 5–20.
Hughes, M. G., and D. A. Robinson, 1996: Historical snow cover variability in the Great Plains region of the USA: 1910 through to 1993. *Int. J. Climatol.,* **16,** 1005–1018.
Hulme, M., 1995: Estimating global changes in precipitation. *Weather,* **50,** 34–42.
——, T. J. Osborn, and T. C. Johns, 1998: Precipitation sensitivity to global warming: Comparison of observations with HadCM2 simulations. *Geophys. Res. Lett.,* **25,** 3379–3382.
Idso, S. B., and A. J. Brazel, 1984: Rising atmospheric carbon dioxide concentrations may increase streamflow. *Nature,* **312,** 51–53.
Jones, P. D., 1994: Hemispheric surface air temperature variations: A reanalysis and an update to 1993. *J. Climate,* **7,** 1794–1802.
——, and M. Hulme, 1996: Calculating regional climatic time series for temperature and precipitation: Methods and illustrations. *Int. J. Climatol.,* **16,** 361–377.
Kalnay, E., and Coauthors, 1996: The NCEP/NCAR 40-Year Reanalysis Project. *Bull. Amer. Meteor. Soc.,* **77,** 437–471.
Karl, T. R., 1998: Regional trends and variations of temperature and precipitation. *The Regional Impacts of Climate Change: An Assessment of Vulnerability,* R. T. Watson, M. C. Zinyowera, and R. H. Moss, Eds., Cambridge University Press, 411–425.
——, and W. R. Knight, 1998: Secular trends of precipitation amount, frequency, and intensity in the United States. *Bull. Amer. Meteor. Soc.,* **79,** 231–241.
Kendall, M. G., 1975: *Rank Correlation Methods.* Charles Griffin, 202 pp.
Kimball, J. S., S. W. Running, and R. R. Nemani, 1997: An improved method for estimating surface humidity from daily minimum temperature. *Agric. For. Meteor.,* **85,** 87–98.
Lettenmaier, D. P., 1975: Detection of trends in water quality data from records with dependent observations. *Water Resour. Res.,* **12,** 1037–1046.
——, E. F. Wood, and J. R. Wallis, 1994: Hydro-climatological trends in the continental United States, 1948–88. *J. Climate,* **7,** 586–607.
Liang, X., D. P. Lettenmaier, E. F. Wood, and S. J. Burges, 1994: A simple hydrologically based model of land surface water and energy fluxes for general circulation models. *J. Geophys. Res.,* **99,** 14 415–14 428.
——, ——, and ——, 1996: One-dimensional statistical dynamic representation of subgrid spatial variability of precipitation in the two-layer variable infiltration capacity model. *J. Geophys. Res.,* **101,** 21 403–21 422.
Lins, H. F., and J. R. Slack, 1999: Streamflow trends in the United States. *Geophys. Res. Lett.,* **26,** 227–230.
Lohmann, D., R. Notle-Holube, and E. Raschke, 1996: A large-scale horizontal routing model to be coupled to land surface parameterization schemes. *Tellus,* **48A,** 708–721.
——, E. Raschke, B. Nijssen, and D. P. Lettenmaier, 1998a: Regional scale hydrology. I. Formulation of the VIC-2L model coupled to a routing model. *Hydrol. Sci. J.,* **43,** 131–141.
——, and Coauthors, 1998b: The Project for Inter-comparison of Land-surface Parameterization Schemes (PILPS) Phase 2(c) Red–Arkansas River Basin experiment. 3. Spatial and temporal analysis of water fluxes. *Global Planet. Change,* **20,** 161–179.
Mann, H. B., 1945: Non-parametric test against trend. *Econometrika,* **13,** 245–259.
Maurer, E. P., G. M. O'Donnell, D. P. Lettenmaier, and J. O. Roads, 2001: Evaluation of the land surface water budget in NCEP/NCAR and NCEP/DOE reanalyses using an off-line hydrologic model. *J. Geophys. Res.,* **106,** 17 841–17 862.
McCabe, G. J., Jr., and D. M. Wolock, 1997: Climate change and the detection of trends in annual runoff. *Climate Res.,* **8,** 129–134.
McCarthy, J. J., O. F. Canziani, N. A. Leary, D. J. Dokken, and K. S. White, Eds., 2001: *Climate Change 2001: Impacts, Adaptation and Vulnerability.* Cambridge University Press, 1000 pp.
Meehl, G. A., F. Zwiers, J. Evans, T. Knutson, L. Mearns, and P. Whetton, 2000: Trends in extreme weather and climate events: Issues related to modeling extremes in projections of future climate change. *Bull. Amer. Meteor. Soc.,* **81,** 427–436.
Milly, P. C. D., R. T. Wetherald, K. A. Dunne, and T. L. Delworth, 2002: Increasing risk of great floods in a changing climate. *Nature,* **415,** 514–517.
Mitosek, H. T., 1995: Climate variability and change within the discharge time series: A statistical approach. *Climatic Change,* **29,** 101–116.
Morel, P., 2001: Why GEWEX? The agenda for a global energy and water cycle research program. *GEWEX News,* Vol. 11, No. 1, 7–11.
Myneni, R. B., R. R. Nemani, and S. W. Running, 1997: Estimation of global leaf area index and absorbed PAR using radiative transfer models. *IEEE Trans. Geosci. Remote Sens.,* **35,** 1380–1393.
Nijssen, B., D. P. Lettenmaier, X. Liang, S. W. Wetzel, and E. F. Wood, 1997: Streamflow simulation for continental-scale river basins. *Water Resour. Res.,* **33,** 711–724.
——, G. M. O'Donnell, D. P. Lettenmaier, D. Lohmann, and E. F. Wood, 2001a: Predicting the discharge of global rivers. *J. Climate,* **14,** 3307–3323.
——, R. Schnur, and D. P. Lettenmaier, 2001b: Global retrospective estimation of soil moisture using the Variable Infiltration Capacity land surface model, 1980–93. *J. Climate,* **14,** 1790–1808.
Richards, G. R., 1993: Change in global temperature: A statistical analysis. *J. Climate,* **6,** 546–559.
Robock, A., Y. V. Konstantin, G. Srinivasan, J. K. Entin, S. E. Hollinger, N. A. Speranskaya, S. Liu, and A. Namkhai, 2000: The global soil moisture data bank. *Bull. Amer. Meteor. Soc.,* **81,** 1281–1299.
Row, L. W., D. A. Hastings, and P. K. Dunbar, 1995: *TerrainBase Worldwide Digital Terrain Data Documentation Manual.* CD-ROM Release 1.0, National Geophysical Data Center, Boulder, CO.
Theil, H., 1950: A rank-invariant method of linear and polynomial regression analysis. *Indagationes Math.,* **12,** 85–91.
Thornton, P. E., and S. W. Running, 1999: An improved algorithm for estimating incident daily solar radiation from measurements of temperature, humidity, and precipitation. *Agric. For. Meteor.,* **93,** 211–228.
Washington, W. M., and Coauthors, 2000: Parallel climate model (PCM) control and transient simulations. *Climate Dyn.,* **16,** 755–774.
WCRP, 1990: The Global Precipitation Climatology Project—Implementation and data management plan. WMO Tech. Doc. 367, Geneva, Switzerland, 47 pp. and appendixes.
Wigley, T. M. L., and P. D. Jones, 1981: Detecting CO_2-induced climate change. *Nature,* **292,** 205–208.
——, and ——, 1985: Influences of precipitation changes and direct CO_2 effects on streamflow. *Nature,* **314,** 149–152.
Wood, E. F., D. P. Lettenmaier, X. Liang, B. Nijssen, and S. W. Wetzel, 1997: Hydrological modeling of continental-scale basins. *Annu. Rev. Earth Planet. Sci.,* **25,** 279–300.
Woodward, W. A., and H. L. Gray, 1993: Global warming and the problem of testing for trend in time series data. *J. Climate,* **6,** 953–962.
Xie, P. P., and P. A. Arkin, 1997: Global precipitation: A 17-year monthly analysis based on gauge observations, satellite estimates, and numerical model outputs. *Bull. Amer. Meteor. Soc.,* **78,** 2539–2557.
Zhang, X. B., K. D. Harvey, W. D. Hogg, and T. R. Yuzyk, 2001: Trends in Canadian streamflow. *Water Resour. Res.,* **37,** 987–998.
Zheng, X., and R. E. Basher, 1999: Structural time series models and trend detection in global and regional temperature series. *J. Climate,* **12,** 2347–2358.